3. Yao, T.-P., Segraves, W. A., Oro, A. E., McKeown, M. & Evans, R. M. *Drosphila* ultraspiracle modulates ecdysone receptor function via heterodimer formation. *Cell* **71,** 63–72 (1992).
4. Thomas, H. E., Stunnenberg, H. G. & Stewart, A. F. Heterodimerization of the *Drosophila* ecdysone receptor with retinoid X receptor and ultraspiracle. *Nature* **362,** 471–475 (1993).
5. Yao, T.-P. *et al.* Functional ecdysone receptor is the product of EcR and ultraspiracle genes. *Nature* **366,** 476–479 (1993).
6. Wurtz, J.-M. *et al.* A new model for 20-hydroxyecdysone and dibenzoylhydrazine binding: A homology modeling and docking approach. *Protein Sci.* **9,** 1073–1084 (2000).
7. Kasuya, K. *et al.* Binding mode of ecdysone agonists to the receptor: comparative modeling and docking studies. *J. Mol. Model.* **9,** 58–65 (2003).
8. Dhadialla, T. S., Carlson, G. R. & Le, D. P. New insecticides with ecdysteroidal and juvenile hormone activity. *Annu. Rev. Entomol.* **43,** 545–569 (1998).
9. Toya, T., Fukasawa, H., Masui, A. & Endo, Y. Potent and selective partial ecdysone agonist activity of chromafenozide in Sf9 cells. *Biochem. Biophys. Res. Commun.* **292,** 1087–1091 (2002).
10. Gampe, R. T. Jr *et al.* Asymmetry in the PPARγ/RXRα crystal structure reveals the molecular basis of heterodimerization among nuclear receptors. *Mol. Cell* **5,** 545–555 (2000).
11. Bourguet, W. *et al.* Crystal structure of a heterodimeric complex of RAR and RXR ligand-binding domains. *Mol. Cell* **5,** 289–298 (2000).
12. Svensson, S. *et al.* Crystal structure of the heterodimeric complex of LXRα and RXRβ ligand-binding domains in a fully agonistic conformation. *EMBO J.* **22,** 4625–4633 (2003).
13. Billas, I. M. L., Moulinier, L., Rochel, N. & Moras, D. Crystal structure of the ligand binding domain of the ultraspiracle protein USP, the ortholog of RXRs in insects. *J. Biol. Chem.* **276,** 7465–7474 (2001).
14. Clayton, G. M., Peak-Chew, S. Y., Evans, R. M. & Schwabe, J. W. The structure of the ultraspiracle ligand-binding domain reveals a nuclear receptor locked in an inactive conformation. *Proc. Natl Acad. Sci. USA* **98,** 1549–1554 (2001).
15. Horlein, A. J. *et al.* Ligand-independent repression by the thyroid hormone receptor mediated by a nuclear receptor co-repressor. *Nature* **377,** 397–404 (1995).
16. Rochel, N., Wurtz, J.-M., Mitschler, A., Klaholz, B. P. & Moras, D. The crystal structure of the nuclear receptor of vitamin D bound to its natural ligand. *Mol. Cell* **5,** 173–179 (2000).
17. Henrich, V. C. & Brown, N. E. Insect nuclear receptors: A developmental and comparative perspective. *Insect Biochem. Mol. Biol.* **25,** 881–897 (1995).
18. Gilbert, L. I., Rybczynski, R. & Warren, J. T. Control and biochemical nature of the ecdysteroidogenic pathway. *Annu. Rev. Entomol.* **47,** 883–916 (2002).
19. Baker, K. D., Warren, J. T., Thummel, C. S., Gilbert, L. I. & Mangelsdorf, D. J. Transcriptional activation of the *Drosophila* ecdysone receptor by insect and plant ecdysteroids. *Insect Biochem. Mol. Biol.* **30,** 1037–1043 (2000).
20. Mohammed-Ali, A. K., Chan, T.-H., Thomas, A. W., Strunz, G. M. & Jewett, B. Structure-activity relationship study of synthetic hydrazines as ecdysone agonists in the control of spruce budworm (*Choristoneura fumiferana*). *Can. J. Chem.* **73,** 550–557 (1995).
21. Hu, X., Cherbas, L. & Cherbas, P. Transcription activation by the ecdysone receptor (EcR/USP): Identification of activation functions. *Mol. Endocrinol.* **17,** 716–731 (2003).
22. Kumar, M. B., Fujimoto, T., Potter, D. W., Deng, Q. & Palli, S. R. A single point mutation in ecdysone receptor leads to increased ligand specificity: Implications for gene switch applications. *Proc. Natl Acad. Sci. USA* **99,** 14710–14715 (2002).
23. Farnegardh, M. *et al.* The three dimensional structure of the liver X receptor beta reveals a flexible ligand binding pocket that can accommodate fundamentally different ligands. *J. Biol. Chem.* **40,** 38821–38828 (2003).
24. Arbeitman, M. N. & Hogness, D. S. Molecular chaperones activate the *Drosophila* ecdysone receptor, an RXR heterodimer. *Cell* **101,** 67–77 (2000).
25. Egea, P. F. *et al.* Crystal structure of the human RXRα ligand-binding domain bound to its natural ligand 9-cis retinoic acid. *EMBO J.* **19,** 2592–2601 (2000).
26. Kissinger, C. R., Gehlhaar, D. K. & Fogel, D. B. Rapid automated molecular replacement by evolutionary search. *Acta Crystallogr. D* **55,** 484–491 (1999).
27. Brünger, A. T. *et al.* Crystallography & NMR system: A new software suite for macromolecular structure determination. *Acta Crystallogr. D* **54,** 905–921 (1998).
28. Jones, T. A., Zou, J. Y., Cowan, S. W. & Kjeldgaard, M. Improved methods for building protein models in electron density maps and the location of errors in these models. *Acta Crystallogr. A* **47,** 110–119 (1991).
29. Greiner, E. F. *et al.* Functional analysis of retinoid Z receptor beta, a brain-specific nuclear orphan receptor. *Proc. Natl Acad. Sci. USA* **93,** 10105–10110 (1996).
30. Potier, N. *et al.* Using non denaturing mass spectrometry to detect fortuitous ligands in orphan nuclear receptors. *Protein Sci.* **12,** 725–733 (2003).

Supplementary Information accompanies the paper on **www.nature.com/nature**.

Acknowledgements We are grateful to G. Holmwood, K. Tietjen and M. Schindler (Bayer CropScience) for providing us with BYI06830 and ponA. We thank H. Greschik, H. Gronemeyer, B. Klaholz and G. Richards for critical comments on the manuscript; Y. Brelivet and J. M. Wurtz for discussion and advice; H. Nierengarten for mass spectrometry analysis; V. Chavant, D. Rose and F. Zink for technical assistance; S. Sasorith for her help with figures; and C. Massobrio for support and encouragement. We thank the staff of the ESRF ID14 beamline (Grenoble, France) and of the French beamline BM30A (Grenoble, France) for assistance during synchrotron data collection. This work was supported by Bayer CropScience and by grants from CNRS, INSERM, the Hôpital Universitaire de Strasbourg, the Ministère de la Recherche et de la Technologie (Programme de Génomique Structurale) and EU-SPINE.

Competing interests statement The authors declare that they have no competing financial interests.

Correspondence and requests for materials should be addressed to D.M. (moras@igbmc.u-strasbg.fr). Atomic coordinates have been deposited in the Protein Data Bank under accession codes 1R1K and 1R20.

Crystal structure of a zinc-finger–RNA complex reveals two modes of molecular recognition

Duo Lu, M. Alexandra Searles & Aaron Klug

Medical Research Council (MRC) Laboratory of Molecular Biology, Cambridge CB2 2QH, UK

Zinc-finger proteins of the classical Cys_2His_2 type are the most frequently used class of transcription factor and account for about 3% of genes in the human genome[1,2]. The zinc-finger motif was discovered[3] during biochemical studies on the transcription factor TFIIIA, which regulates the 5S ribosomal RNA genes of *Xenopus laevis*[4,5]. Zinc-fingers mostly interact with DNA, but TFIIIA binds not only specifically to the promoter DNA, but also to 5S RNA itself[6–9]. Increasing evidence indicates that zinc-fingers are more widely used to recognize RNA[10–13]. There have been numerous structural studies on DNA binding[14], but none on RNA binding by zinc-finger proteins. Here we report the crystal structure of a three-finger complex with 61 bases of RNA, derived[15] from the central regions of the complete nine-finger TFIIIA–5S RNA complex. The structure reveals two modes of zinc-finger binding, both of which differ from that in common use for DNA: first, the zinc-fingers interact with the backbone of a double helix; and second, the zinc-fingers specifically recognize individual bases positioned for access in otherwise intricately folded 'loop' regions of the RNA.

The classical zinc-finger motif consists of a sequence of about 30 amino acids containing two histidines, two cysteines and three hydrophobic residues, which are all at conserved positions (Fig. 1b). It forms a small, independently folded domain stabilized by Zn^{2+}, which can be used repeatedly in a modular fashion to achieve sequence-specific recognition of DNA[3]. The domains all have the same structural framework, but achieve chemical distinctiveness through variations in key residues. Structurally, the domain is composed of a β-hairpin and an α-helix pinned together by Zn^{2+}. In the canonical Zif268 docking arrangement, the primary contacts are made by the α-helix, which binds in the DNA major groove through primary hydrogen-bond interactions from helical positions −1, 3 and 6 to one strand of the DNA, and through a secondary interaction from helical position 2 to the other strand[14]. There are, however, wide variations in this arrangement among the known zinc-finger–DNA complexes.

Thus, DNA binding is well understood, but the molecular basis of recognition of RNA by zinc-fingers has remained elusive. The secondary and tertiary structure of RNA is more complex than that of DNA, comprising internal loops and helical elements closed by hairpin loops. But much has been learned about the binding of TFIIIA to 5S RNA through chemical, biochemical and mutagenesis studies[16–20]. In particular, the locations of the nine fingers have been mapped with respect to the secondary RNA structure, and also their relative contributions to the overall binding affinity have been determined. The most important region of the 5S RNA is the central half of the molecule comprising loop E, helix V, loop A, helix II and part of helix IV. Accordingly, the most important part of the TFIIIA protein for RNA binding is the central set of fingers 4–7, with the major contribution coming from fingers 4–6 (see Table 1 in ref. 15).

Ideally what is required is an X-ray structure of the complete complex of TFIIIA and 5S RNA, which occurs naturally as a 7S ribonucleoprotein storage particle[6]. But as our attempts to crystallize this, or a reconstituted complex, have failed, we have produced subcomplexes[15] between the essential parts: namely, the central

 © 2003 Nature Publishing Group

region of the RNA and fingers 4–6 and/or 4–7. We have checked by RNA footprinting[15] that these three- and four-finger peptides have the same structural relationship to the RNA as they do when they are part of a complete nine-finger protein.

A complex of a truncated 5S RNA with 61 bases (5S RNA 61n) and a three-finger peptide (Fig. 1a, b) diffracted to 3 Å resolution, and we have solved this structure (Fig. 1c). The asymmetric unit contains two complexes of the three-finger peptide and RNA, and an additional peptide molecule with only two of its three fingers ordered. This additional peptide is a 'passenger' in the open crystal structure, making contacts with the outer faces of fingers 4 and 5 in one complex away from the RNA. It is not involved in the specific interaction. The two non-crystallographically related complexes are folded in the same way, with the exception of helix I in the second complex, which is bent slightly differently with respect to the rest of the RNA molecule. Because helix I has no part in the interaction with the three-finger peptide, our conclusions are not affected.

The overall structure of the complex and the geometry of the binding between peptide and RNA is shown in Figs 1d and 2a. As expected from biochemical studies[16–20], finger 4 binds to loop E, finger 5 to helix V, and finger 6 to loop A. The hydrogen-bond interactions between peptide and RNA are shown in Fig. 2b. The distances in Fig. 2c indicate hydrogen bonds, but some of these may be mediated by water, which cannot be determined at the current resolution. The space-filling model (Fig. 1d) shows how the close packed fingers curl around the long axis of the RNA. The spatial relationship (Fig. 2a) between fingers 4 and 5 is similar to that in the complex with DNA[21], but that between 5 and 6 is different. Both spatial relationships differ from those between fingers in the canonical Zif268–DNA structure and other complexes[14]. Allowing for the fact that helix V has 1 base pair less in *Xenopus* 5S RNA than in archaebacteria, the RNA structure closely resembles that in the 50S ribosomal subunit[22] of *Haloarcula marismortui*, as expected from the large amount of conserved sequence.

The structure of loop E is shown in Fig. 3a. It is intricately folded and also structurally rigid, held by various hydrogen bonds and base stacking. The strands, as depicted in the secondary structure, cross over and are stabilized by reciprocal purine stacking: 75G on 99G, and 100A on 77A. Base 75G protrudes outward and is held by a hydrogen bond to 76U, which forms a base triple with A100, as first recognized in an NMR study of loop E (ref. 23). Several of the

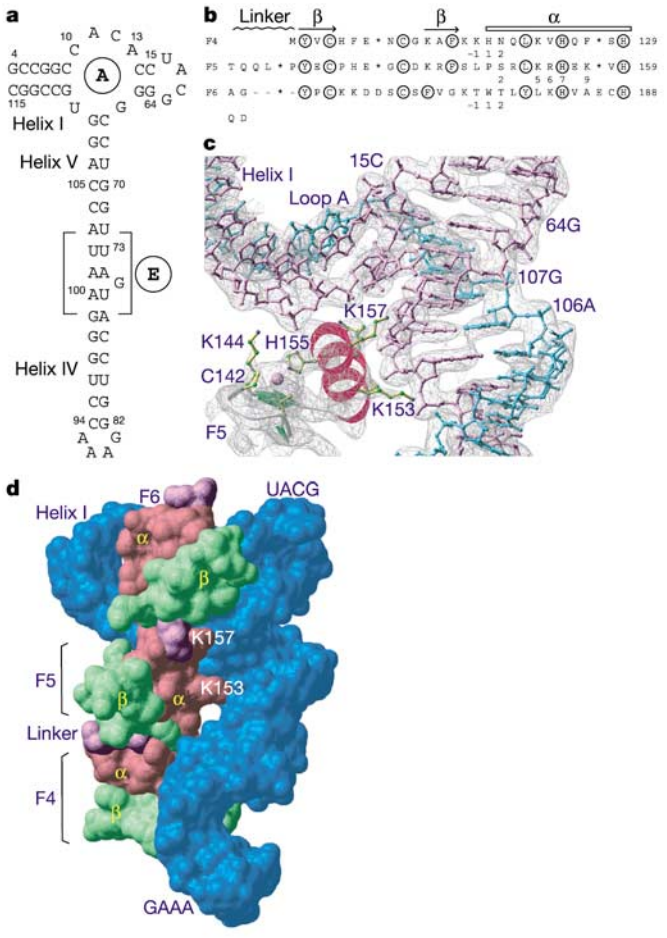

Figure 1 Components of the zinc-finger–RNA complex. **a**, Secondary structure of 5S RNA 61n, the truncated RNA. Loops A and E are circled and helices are indicated by roman numerals. **b**, Sequence of the central three-finger peptide from TFIIIA. Some helical positions are indicated. Conserved residues are circled[3], but the alignment in the atypical finger 6 (F6) has been revised according to the structure. **c**, Portion of the electron density map. The RNA is shown as a ball-and-stick model, and finger 5 as a ribbon model. **d**, Space-filling model calculated with a radius of 1.5 Å. RNA is shown in blue, β-sheets in green, α-helices in red, and linkers in purple. The buried surface area is 1,860 Å^2.

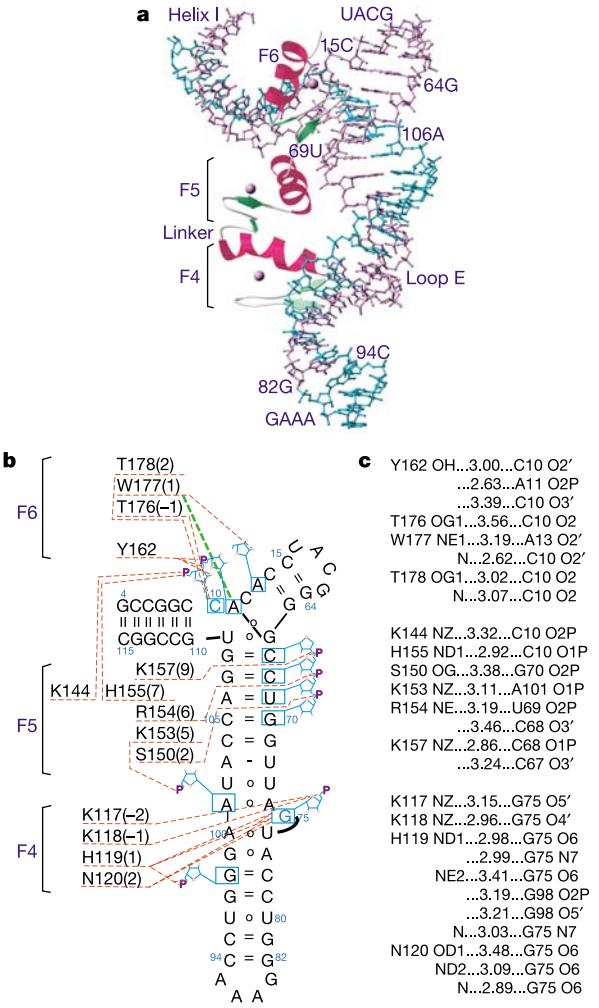

Figure 2 Interactions of the three-finger peptide with the RNA. **a**, Overall view of the complex of TFIIIA(4–6) and 5S RNA 61n. The RNA is represented as a ball-and-stick model with nucleotides 4–82 in purple and nucleotides 83–115 in blue, and the protein is shown as a ribbon model. Purple balls represent zinc ions. **b**, Hydrogen-bond interactions between protein and RNA. Amino acid helical positions in brackets. Nucleotides involved in interactions are boxed, and bases shown in blue make direct interactions with protein. The broken green line indicates stacking of aromatic rings. **c**, List of hydrogen-bond interactions for each of the three fingers.

© 2003 Nature Publishing Group

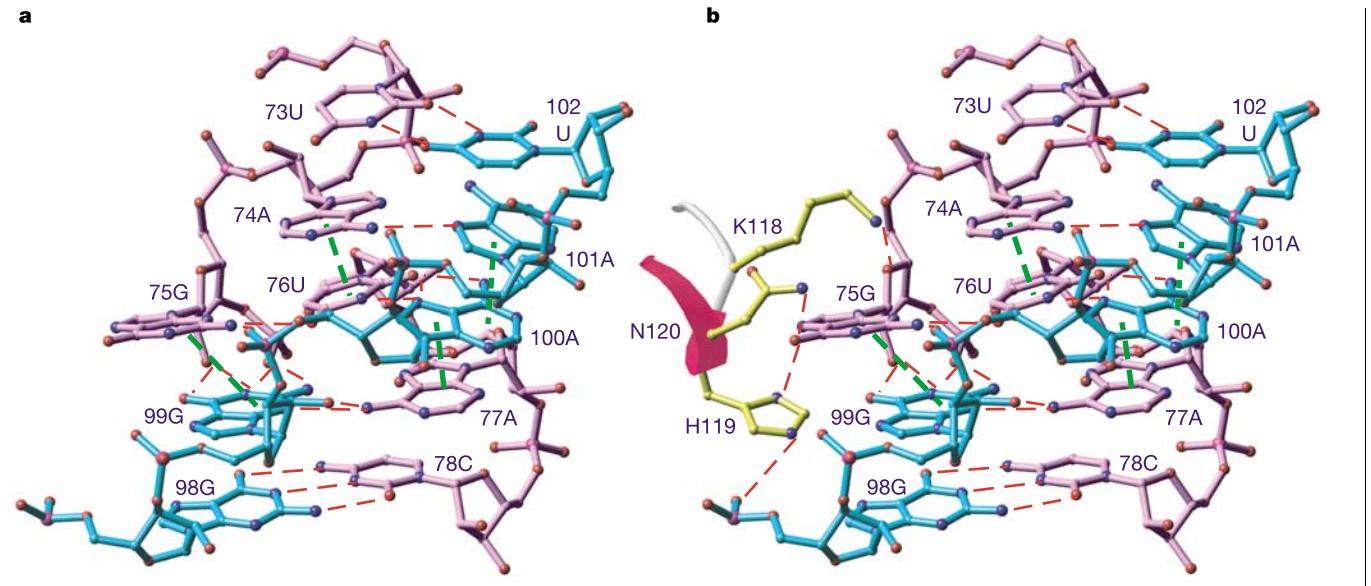

Figure 3 Recognition of loop E by finger 4. **a**, Structure of loop E. The chains are coloured as in Fig. 2a. Hydrogen bonds are shown in red, and base stacking in green. Stacking interactions are assigned according to the degree of overlap and have separation distances shorter than 3.8 Å. **b**, Interaction of loop E with the N terminus of the helix of finger 4. Colours are the same as in **a**, with peptide side chains in yellow. The hydrogen-bond interactions between protein and RNA are listed in Fig. 2c. The bulged base 75G is gripped by hydrogen bonds from Asp 120 and His 119, and its ribose by a hydrogen bond from Lys 118.

hydrogen-bond interactions were deduced from a detailed mutagenesis study[20]. This type of structural element has been found in other ribosomal RNAs, where it has been called a "G-bulged cross strand stack"[24].

The interactions of loop E with finger 4 are shown in Fig. 3b and listed in Fig. 2c. The bulged base 75G is gripped by hydrogen bonds from Asp 120 and His 119 in positions 2 and 1, respectively, at the amino terminus of the recognition helix, and the ribose of the nucleotide is hydrogen-bonded to Lys 118 in position −1. Thus, the very tip of the helix is used for this specific base recognition. The importance of 75G has long been known because if it is deleted[18], or mutated[20], *in vitro* binding to TFIIIA is markedly reduced. Quantitative mutagenesis studies[19] show that there is a 30-fold reduction in affinity when Lys 118 is replaced by alanine, and a 77-fold reduction when both Lys 118 and Asp 120 are replaced, thereby corroborating our structure.

In terms of the interaction of finger 6 with loop A, what is depicted as a loop in the RNA secondary structure is a complex three-way junction between three RNA helices: V, I and II. At the ends of each of the three helices abutting the loop are two G•C base pairs, which form the rigid pillars of a complex fold (Fig. 4a). The backbone from nucleotides 10–13 follows an extended path, making a sharp 'S' bend to join the double helix at nucleotide 14. These four residues form an inner subsidiary loop, closed by the stacking of

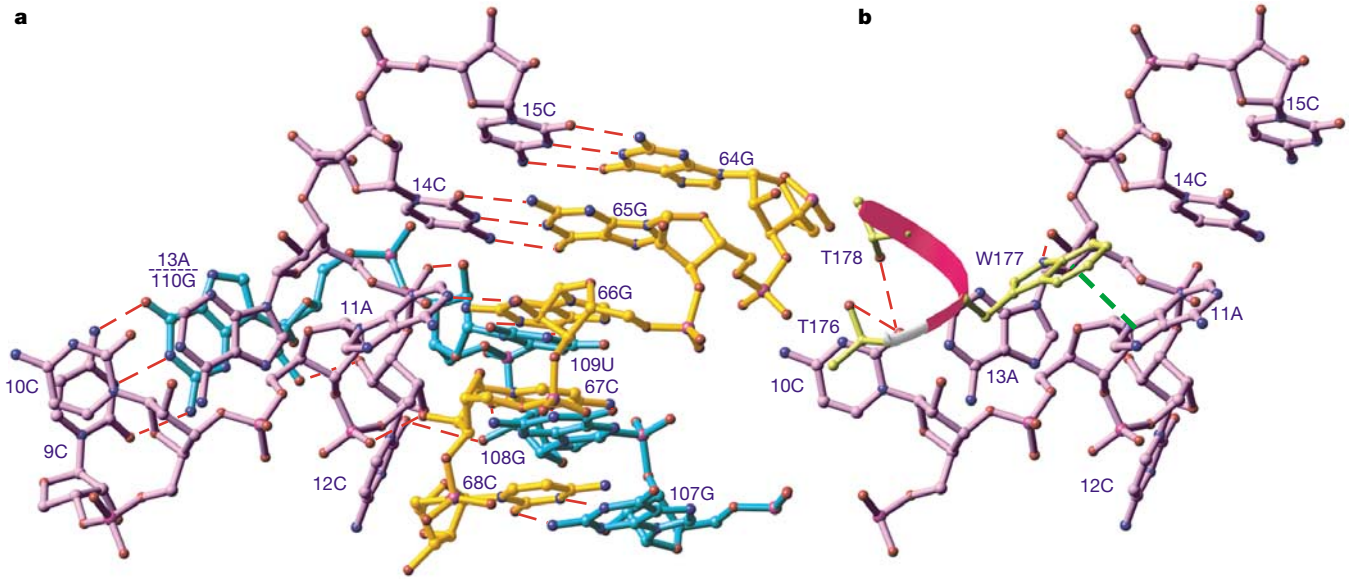

Figure 4 Recognition of loop A by finger 6. **a**, Structure of loop A. Three colours are used to indicate the three-way junction, blue and purple as in Figs 2 and 3, but with nucleotides 64–68 in orange. **b**, Interaction of loop A with the N terminus of the helix of finger 6. Peptide side chains are shown in yellow. The ring of Trp 177 docks on the face of base 11A, and the two flanking residues, Thr 176 and Thr 178, make hydrogen bonds to base 10C. Trp 177 also makes a hydrogen bond to the ribose of 13A.

© 2003 Nature Publishing Group

13A on 110G, that is hydrogen-bonded to base 9C, which in turn stacks under 10C. Base 11A protrudes outward, fixed by a hydrogen bond to 66G, which forms a base triple with 109U. The face of base 11A is exposed on the outside of the RNA (Fig. 4b).

The binding of finger 6, as in the case of finger 4, involves the N terminus of its recognition helix. Indeed, the same positions at the tip of the helix are involved: namely, −1, 1 and 2, which are occupied here by Thr 176, Trp 177 and Thr 178, respectively (Fig. 4b). The ring of Trp 177 stacks on the face of the exposed base 11A, and the two flanking threonines makes hydrogen bonds to base 10C. Trp 177 also makes a hydrogen bond to the ribose of 13A. Again, there is good agreement with biochemical and mutagenesis studies. The aromatic character of Trp 177, the basis of its stacking, has been reported to be essential for 5S RNA recognition because it can be replaced by phenylalanine but not by alanine[20]. Of the conserved stretch from 10C to 13A, only one position can be occupied by another base, namely 12C (ref. 20). This is because the base points away from the binding site (Fig. 4b). Alanine substitution of Thr 176 and Thr 178 leads to a 38-fold reduction in binding affinity[19].

The interaction of finger 5 with the RNA differs from the specific base contacts made by fingers 4 and 6. The interaction is made almost completely by multiple contacts of basic amino acid residues with the phosphate backbone (Fig. 2c): two of these, Lys 153 and Lys 157, straddle the major groove of the RNA (Fig 1c, d). The α-helix of the finger is still used to provide the contacting residues, but these emanate predominantly from the lower part of the helix towards the C terminus. Support for this conclusion comes from alanine mutagenesis of the helical positions involved in DNA binding, which show little effect[19]. Strong corroborating evidence for the involvement of the backbone phosphates comes from ethylation interference assays[20]. Indeed, it is remarkable that these previous biochemical studies succeeded in identifying many of the essential moieties in both protein and RNA.

The interaction of finger 5 with the double-stranded RNA of helix V is distinct from that with the DNA double helix[21]. The base sequence of RNA helix V is identical (except for U replacing T) with that of the parent DNA double helix, so that finger 5 might have been expected to bind in a similar manner. This does not happen, presumably because the major groove of the RNA double helix is too deep to be penetrated by the α-helix. The α-helix is still used and provides nonspecific contacts to the phosphate sugar backbone. Presumably, the register of the run of fingers with the RNA is decided by the specific base contacts made by fingers 4 and 6, restricting finger 5 to bind to the RNA double helix in between. Finger 5 therefore seems to be a nonspecific spacer element that, through backbone contacts, contributes substantially to the binding affinity. This situation is reciprocal to the way in which the three-finger peptide associates with DNA[21], where finger 5 makes specific contacts and fingers 4 and 6 act as non-binding spacers.

The dual role of finger 5 binding to DNA and RNA in different ways points to the wide difference between these molecules. The primary interaction of fingers with DNA is base recognition. The DNA double helix is essentially regular, despite small, local, sequence-dependent variations, thus the specificity of recognition lies in a particular sequence of bases. By contrast, RNA molecules form complex structures comprising internal 'loops' and double helices, which are sometimes closed by hairpin loops. The general conclusion from our work is that the zinc-finger domain can be used to recognize all of these different elements. It can recognize RNA specifically by contacts with individual bases that are exposed for access out of a structurally rigid, complicated fold. At the same time, the zinc-finger architecture is versatile enough to provide binding in another mode to a regularly folded double-helical region, where it is the structure rather than the sequence that is recognized. Thus, the finger 5 interaction may account for other instances of specific binding by zinc-fingers to double-stranded RNA that is not sequence dependent[11,12]. It will be interesting to compare zinc-finger usage more generally with other types of RNA-binding protein. A diverse set of structures is known, but so far there is no comprehensive library of interactions, including those from the structures of the ribosomal units.

The adaptability of the zinc-finger for molecular recognition is further attested to by increasing evidence for the use of zinc-fingers in protein–protein recognition; for example, the six-finger protein Aiolos uses two of its fingers to bind to another zinc-finger Ikaros and the remaining four for binding DNA[25]. In addition, it seems that zinc-fingers are still rapidly evolving[2], presumably because, as small self contained modules, they can be easily passed on in exon shuffling. There is more to be learned. □

Methods

Reconstitution of zinc-finger–RNA complex

RNA and protein were prepared as described[15]. RNA and protein samples were always freshly refolded and trial binding was carried out before the bulk reconstitution of complex. Binding affinity can vary slightly between different batches of protein: the molar ratio of RNA to protein is 1:1 normally and 1:2 in extreme cases. Extra protein was added in bulk preparations to secure 100% of bound RNA.

We mixed the RNA and protein in dilute concentrations (~4.7 μM) to avoid irreversible precipitation. The mixture was then dialysed against binding buffer (20 mM HEPES pH 7.0, 150 mM KCl, 1.5 mM $MgCl_2$, 5 mM dithiothreitol (DTT) and 0.1 mM $ZnSO_4$) at 4 °C overnight. A white precipitate of aggregated protein normally appeared and was removed by ultracentrifugation at 55,000 r.p.m., 4 °C, 30 min. The supernatant was concentrated in a Vivaspin concentration unit (Vivascience) to a final concentration of 5 mg ml^{-1}.

Crystallization

The 5S RNA 61n construct was designed with two different tetraloops capping the stem loops. The particular choice of the two tetraloops (Fig. 1a) differs from that shown in Fig. 4 of ref. 15, because it was found to be essential for crystallization of the complex.

Crystallization was carried out by the hanging-drop evaporation method at 4 °C. Concentrated complex was mixed with reservoir buffer (20% PEG 8,000, 200 mM KCl, 5 mM $MgCl_2$, 50 mM MES, (pH 5.6), 3 mM DTT and 0.3 mM $ZnSO_4$) at a 1:1 volume ratio. Flexible needles normally appeared in 2 d. Very occasionally, block-shaped crystals appeared after 2 weeks. These were used for seeding, and block-shaped crystals were reproduced after 2–3 d. We checked the composition of crystal batches by gel electrophoresis.

Data collection

Crystals were soaked in increasing steps of 30 min each into cryo-protection buffer containing 18% ethylene glycol: 5% in the first three steps and 3% in the last step. A crystal held in a loop was frozen by dipping it directly into liquid nitrogen.

The crystals diffracted close to 3 Å resolution in space group *C*2, with cell dimensions of $a = 58.6$ Å, $b = 191.6$ Å, $c = 79.8$ Å and $\beta = 101.5°$. Two-wavelength multiple anomalous dispersion (MAD) data sets at the zinc absorption edge were collected at beam line BM30A of the European Synchrotron Radiation Facility (ESRF), Grenoble. The data set at the peak wavelength of 1.28200 Å was collected to 3.2 Å, and that at the inflection wavelength of 1.28347 Å was collected to 3.3 Å. Subsequently, we collected a slightly higher resolution data set to 3.1 Å at beam line ID14.2 of the Synchrotron Radiation Source, Daresbury, UK.

Structure determination

Data sets were processed with MOSFLM and scaled with SCALA in the CCP4 suite[26]. Data sets collected at the peak wavelength and the inflection wavelength, and the high resolution gave an R_{merge} of 6.9%, 6.6% and 5.1%, respectively. The first zinc sites were obtained by SHELX[27] and were refined in SHARP[28]. SHARP produced a clear experimental phasing map with a solvent content of 50%.This showed in the asymmetric unit the presence of two complexes and one extra protein molecule with only two of its fingers ordered. We built a model of one of the complexes manually using the program O (ref. 29), and searched out the second complex out by using the model of the first complex with the program MOLREP in the CCP4 package[26]. The extra two ordered fingers were built manually in O. The whole asymmetric unit was first refined with Refmac5 in the CCP4 package[26] to reach values of $R_{free} = 30\%$ and $R_{work} = 20\%$; the refinement was then transferred to CNS[30] to reach final values of $R_{free} = 25.6\%$ and $R_{work} = 21.5\%$ (r.m.s. bond length, 0.0067 Å; and r.m.s. bond angle, 1.27°). The Ramachandran plot for the protein shows six residues in the generously allowed regions and only one in the disallowed regions. Figures of the models were drawn in Ribbons.

To check that the extra peptide had no effect on the complex, we solved the structure of another complex with 57 bases of RNA, in which the GAAA tetraloop was removed at the end of helix IV and which produced crystals that diffracted to 3.5 Å resolution. This crystal grew in a different but related space group of *C*222, with a similar cell volume. The asymmetric unit contained only one complex, and the structure was solved by molecular replacement to a value of $R_{free} = 0.4$, but not refined. This showed the same arrangement as the current structure without the extra peptide in first crystal, but we did not proceed with the refinement because of the lower resolution.

© 2003 Nature Publishing Group

Received 1 August; accepted 22 September 2003; doi:10.1038/nature02088.

1. Clamp, M. *et al.* Ensembl 2002: accommodating comparative genomics. *Nucleic Acids Res.* **31,** 38–42 (2003).
2. Bateman, A. *et al.* The Pfam protein families database. *Nucleic Acids Res.* **30,** 276–280 (2002).
3. Miller, J., McLachlan, A. D. & Klug, A. Repetitive zinc-binding domains in the protein transcriptional factor IIIA from *Xenopus* oocytes. *EMBO J.* **4,** 1609–1615 (1985).
4. Sakonju, S. & Brown, D. D. Contact points between a positive transcription factor and the *Xenopus* 5S RNA gene. *Cell* **31,** 395–405 (1982).
5. Engelke, D., Ng, S.-Y., Shastry, B. & Roeder, R. Specific interaction of a purified transcription factor with an internal control region of 5S RNA genes. *Cell* **19,** 717–728 (1980).
6. Picard, B. & Wegnez, M. Isolation of a 7S particle from *Xenopus laevis* oocytes: a 5S RNA–protein complex. *Proc. Natl Acad. Sci. USA* **76,** 241–245 (1979).
7. Pelham, H. & Brown, D. A specific transcription factor that can bind to either the 5S RNA gene or 5S RNA. *Proc. Natl Acad. Sci. USA* **77,** 4170–4174 (1980).
8. Bogenhagen, D. F. & Sands, M. S. Binding of TFIIIA to derivatives of 5S RNA containing sequence substitutions or deletions defines a minimal TFIIIA binding site. *Nucleic Acids Res.* **20,** 2639–2645 (1992).
9. Theunissen, O., Rudt, F., Guddat, U., Mentzel, H. & Pieler, T. RNA and DNA binding zinc fingers in *Xenopus* TFIIIA. *Cell* **71,** 679–690 (1992).
10. Nagai, K. *et al.* Structure and assembly of the spliceosomal snRNPs. *Biochem. Soc. Trans.* **29,** 15–26 (2001).
11. Finerty, P. J. & Bass, B. L. A *Xenopus* zinc finger protein that specifically binds dsRNA and RNA–DNA hybrids. *J. Mol. Biol.* **271,** 195–208 (1997).
12. Mendez-Vidal, C., Wilhelm, M. T., Hellborg, F., Qian, W. & Wiman, K. G. The p53-induced mouse zinc finger protein wig-1 binds double-stranded RNA with high affinity. *Nucleic Acids Res.* **30,** 1991–1996 (2002).
13. Ladomery, M., Sommerville, J., Woolner, S., Slight, J. & Hastie, N. Expression in *Xenopus* oocytes shows that WT1 binds transcriptions *in vivo*, with a central role for zinc finger one. *J. Cell Sci.* **116,** 1539–1549 (2003).
14. Wolfe, S. A., Nekludova, L. & Pabo, C. O. DNA recognition by Cys_2His_2 zinc finger proteins. *Annu. Rev. Biophys. Biomol. Struct.* **29,** 183–212 (2000).
15. Searles, M. A., Lu, D. & Klug, A. The role of the central zinc fingers of transcription factor IIIA in binding to 5S RNA. *J. Mol. Biol.* **301,** 47–60 (2000).
16. Clemens, K. R. *et al.* Molecular basis for specific recognition of both RNA and DNA by a zinc finger protein. *Science* **260,** 530–533 (1993).
17. McBryant, S. J. *et al.* Interaction of the RNA binding fingers of *Xenopus* transcription factor IIIA with specific regions of 5S ribosomal RNA. *J. Mol. Biol.* **248,** 44–57 (1995).
18. Setzer, D. R., Menezes, S. R., del Rio, S., Hung, V. S. & Subramanyan, G. Functional interactions between the zinc fingers of *Xenopus* transcription factor IIIA during 5S rRNA binding. *RNA* **2,** 1254–1269 (1996).
19. Friesen, W. J. & Darby, M. K. Phage display of RNA binding zinc fingers from transcription factor IIIA. *J. Biol. Chem.* **272,** 10994–10997 (1997).
20. Theunissen, O., Rudt, F. & Pieler, T. Structural determinants in 5S RNA and TFIIIA for 7S RNP formation. *Eur. J. Biochem.* **258,** 758–767 (1998).
21. Nolte, R. T., Conlin, R. M., Harrison, S. C. & Brown, R. S. Differing roles for zinc fingers in DNA recognition: structure of a six-finger transcription factor IIIA complex. *Proc. Natl Acad. Sci. USA* **95,** 2938–2943 (1998).
22. Ban, N., Nissen, P., Hansen, J., Moore, P. B. & Steitz, T. A. The complete atomic structure of the large ribosomal subunit at 2.4 Å resolution. *Science* **289,** 905–920 (2000).
23. Wimberley, B., Varani, G. & Tinoco, I. The conformation of loop E in eukaryotic 5S ribosomal RNA. *Biochemistry* **32,** 1078–1087 (1993).
24. Correll, C. C. *et al.* Crystal structure of the ribosomal RNA domain essential for binding elongation factors. *Proc. Natl Acad. Sci. USA* **95,** 13436–13441 (1998).
25. Morgan, B. *et al.* Aiolos, a lymphoid restricted transcription factor that interacts with Ikaros to regulate lymphocyte differentiation. *EMBO J.* **16,** 2004–2013 (1997).
26. Collaborative Computational Project 4, The CCP4 suite: programs for protein crystallography. *Acta Crystallogr. D* **50,** 760–763 (1994).
27. Sheldrick, G. M. & Gould, R. O. Structure solution by iterative peaklist optimization and tangent expansion in space group P1. *Acta Crystallogr. B* **51,** 423–431 (1995).
28. de la Fortelle, E. & Bricogne, G. Maximum-likelihood heavy-atom parameter refinement for multiple isomorphous replacement and multiwavelength anomalous diffraction methods. *Methods Enzymol.* **276,** 472–494 (1997).
29. Jones, T. A., Zou, J-Y., Cowan, S. W. & Kjeldgaard, M. Improved methods for building protein models in electron density maps and the location of errors in these models. *Acta Crystallogr. A* **47,** 110–119 (1991).
30. Brunger, A. T. *et al.* Crystallography & NMR system: a new software suite for macromolecular structure determination. *Acta Crystallogr. D* **54,** 905–921 (1998).

Acknowledgements We acknowledge the Daresbury Laboratory and the ESRF for provision of facilities. We thank P. Evans and other colleagues for advice and help. D.L. was initially supported by a grant from the Human Frontier Science Programme (to A.K.) and later by a Fellowship from the Sino-British Fellowship Trust.

Competing interests statement The authors declare that they have no competing financial interests.

Correspondence and requests for materials should be addressed to A.K. (akl@mrc-lmb.cam.ac.uk). Coordinates are deposited in the Protein Data Bank under accession code 1UN6.

retraction

Hes1 is a target of microRNA-23 during retinoic-acid-induced neuronal differentiation of NT2 cells

Hiroaki Kawasaki & Kazunari Taira

Nature **423**, 838–842 (2003).

In this Article, the messenger RNA that is identified to be a target of microRNA-23 (miR-23) is from the gene termed human 'homolog of ES1' (HES1), accession number Y07572, and not from the gene encoding the transcriptional repressor 'Hairy enhancer of split' HES1 (accession number NM_00524) as stated in our paper. We incorrectly identified the gene because of the confusing nomenclature. The function of HES1 Y07572 is unknown but the encoded protein shares homology with a protein involved in isoprenoid biosynthesis. Our experiments in NT2 cells had revealed that the protein levels of the repressor Hes1 were diminished by miR-23. Although we have unpublished data that suggest the possibility that miR-23 might also interact with Hes1 repressor mRNA, the explanation for the finding that the level of repressor Hes1 protein decreases in response to miR-23 remains undefined with respect to mechanism and specificity. Given the interpretational difficulties resulting from our error, we respectfully retract the present paper. Further studies aimed at clarifying the physiological role of miR-23 will be submitted to a peer-reviewed journal subject to the outcome of our ongoing research. □

addendum

An expressed pseudogene regulates the messenger-RNA stability of its homologous coding gene

Shinji Hirotsune, Noriyuki Yoshida, Amy Chen, Lisa Garrett, Fumihiro Sugiyama, Satoru Takahashi, Ken-ichi Yagami, Anthony Wynshaw-Boris & Atsushi Yoshiki

Nature **423**, 91–96 (2003).

In this Letter, it is shown using transgene insertion mouse mutants that the *Makorin1-p1* pseudogene regulates the expression of its related coding gene. An example has been drawn to our attention of another transcribed pseudogene that regulates the expression of its related coding gene, but by a different mechanism, in the mollusc *Lymnaea stagnalis*[1]. □

1. Korneev, S. A., Park, J.-H. & O'Shea, M. Neuronal expression of neural nitric oxide synthase (nNOS) protein is suppressed by an antisense RNA transcribed from an NOS pseudogene. *J. Neurosci.* **19,** 7711–7720 (1999).

 © 2003 Nature Publishing Group